Proposed design class of grazing incidence echelle spectrometers: critical analysis and reevaluation

Michael C. Hettrick, Patrick Jelinsky, Stuart Bowyer, and Roger F. Malina

Applied Optics Vol. 23, Issue 22, pp. 4058-4066 (1984)

http://dx.doi.org/10.1364/AO.23.004058

Proposed design class of grazing incidence echelle spectrometers: critical analysis and reevaluation

Michael C. Hettrick, Patrick Jelinsky, Stuart Bowyer, and Roger F. Malina

The class of grazing incidence spectrometers proposed by Cash [Appl. Opt. 21, 710 (1982)] and by McClintock and Cash [Proc. Soc. Photo-Opt. Instrum. Eng. 331, 12 (1982)] for use in the extreme and far ultraviolet has been analyzed. We calculate efficiencies which are lower by a factor of 4 than those estimated by the above authors. This discrepancy is due dominantly to their use of incorrect reflectances. We also calculate a factor of 10 smaller bandpass (3%) and a factor of 2 lower spectral resolution ($\lambda/\Delta\lambda \simeq 4000$) at the spectrum edges. These discrepancies are due to underestimated camera mirror aberrations and neglect of echelle ripple considerations. We consider modifications to overcome these limitations. A Wolter-Schwarzschild type-I camera mirror of large radius increases the bandpass by a factor of 10. However, the proposed spectral resolution over this bandpass requires a very long instrument and/or a significant further decrease in efficiency. A sample design consists of a normal incidence camera and a grazing incidence 0.5-sec of arc collecting mirror and delivers $\lambda/\Delta\lambda = 20{,}000$ over a 40% range in wavelength. However, the normal incidence reflection decreases the efficiency by an additional factor of 3, only wavelengths longward of ~400 Å are directly accessible, and the total instrument length is 6.7 m. Such limitations preclude the usefulness of this design class in several applications currently under study in astronomical space instrumentation. Other classes of grazing incidence spectrometers which are not subject to these limitations are being investigated.

I. Introduction

In two publications,[1,2] hereafter denoted as papers 1 and 2, a grazing incidence version of the echelle spectrograph was presented (Fig. 1). It consists of confocal collecting and collimating mirrors, a crossed pair of plane reflection gratings, a camera mirror, and a position-sensitive detector. The high-dispersion echelle grating is mounted in the extreme off plane or conical diffraction mode. The essential motivation for this design is the high diffraction efficiency which can be achieved at grazing incidence in conical diffraction.[3–5]

The use of such instruments to cover the extreme ultraviolet (EUV) and far-ultraviolet (FUV) spectral region $\lambda \simeq 100$–2000 Å is of particular interest in the context of current studies for future orbiting astronomy observatories.[6] Paper 2 specifically addressed this application of the Cash spectrometer design and proposed a "space observatory" including design parameters for the optics. Similar parameters were indicated in paper 1 for an EUV spectrograph design.

To provide useful comparisons between these and other competing designs, it is necessary to consistently employ the same level of analysis in estimating performance characteristics. In Sec. II we report the results of our ray-tracing calculations using the design parameters given in papers 1 and 2. In Sec. III we report the efficiency which results from use of accepted reflectance data. In Sec. IV we indicate several schemes which can improve some of the performance parameters, and in Sec. V we summarize this work.

II. Imaging Performance

The system constraints which ultimately drive the performance of dispersive spectrometers are (1) quality of the collecting mirror or figure (in the case of spectroscopy on diffuse objects, this quantity is replaced by the entrance slit width), (2) physical size of the instrument, and (3) resolvable detector pixel size. For the proposed design class these constraints determine the spectrometer performance in the following manner: (a) The spectrometer length is determined by the diameter of the collecting mirror D and the diameter of the col-

The authors are with University of California, Space Sciences Laboratory, Berkeley, California 94720.

Received 6 September 1983.
0003-6935/84/224058-09$02.00/0.

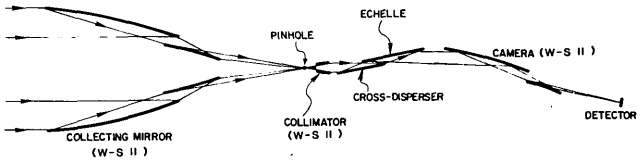

Fig. 1. Schematic diagram of the echelle spectrometer class proposed by Cash. The system contains eight grazing incidence reflections.

limating mirror d. Higher concentration ratios $c \equiv D/d$ result in shorter systems; (b) the collimator dominates the off-axis response of the collecting optics as it lies near the focus. This effect will be neglected, with the star assumed to lie exactly along the optical axis; (c) the blurring of a stellar image due to the collecting mirror figure will be amplified by the concentration ratio c. The resulting nonparallelism or aspect of rays incident to the plane grating system determines the echelle grating dispersion required to obtain a desired spectral resolution $\lambda/\Delta\lambda$; (d) echelle dispersion decreases at shallower reflection angles providing a trade-off between efficiency and resolution; (e) the spectral resolution at the center of the spectrum also depends on the detector pixel size and the camera focal length. At grazing incidence, echelles at high blaze angle distort the incident stellar image into elongated ellipses, driving a longer camera focal length; (f) beam distortion also occurs following echelle diffraction, requiring a large radius camera mirror; (g) the echelle dispersion and the camera field of view jointly specify the value of the echelle order necessary to fit adjacent orders within the field. The detector size is assumed not to be a limiting factor; (h) the cross-dispersion required to separate adjacent echelle orders must also fit within the camera field of view. This sets the number of echelle orders and thus the simultaneous bandpass.

We shall start with the constraints used in papers 1 and 2 for the "all grazing echelle spectrometer." Paper 1 assumed a 1-sec of arc mirror figure, a 4.7-m long instrument (which included a 2.2-m spectrograph) and a pixel size of 15 μm. In the context of future planned astronomy satellites, these constraints are reasonable, but cannot be significantly relaxed. The resulting performance estimates reported in paper 1 were (1) a spectral resolution of $\lambda/\Delta\lambda$ = 10,000, (2) a simultaneous bandpass of 30% in wavelength, and (3) an EUV efficiency of ~4% in collecting area delivered to the detector. Paper 2 assumed a 0.68-sec of arc mirror figure and a pixel size of 20 μm. Summing the values indicated therein for the size of the individual optical elements, we find a total instrument length of ~6 m. The resulting performances were reported to be $\lambda/\Delta\lambda$ = 20,000 over a 15% range in wavelength and an efficiency equal to that estimated in paper 1. Specific parameters for designs tailored to operate at different wavelengths can be found in Tables I and II of paper 2. The diameter of the collecting mirror was taken to be 1 m in both papers.

The proposed all-grazing echelle design class incorporates a Wolter-Schwarzschild (W-S) type-II camera mirror (Fig. 1). To resolve the detector pixels, paper

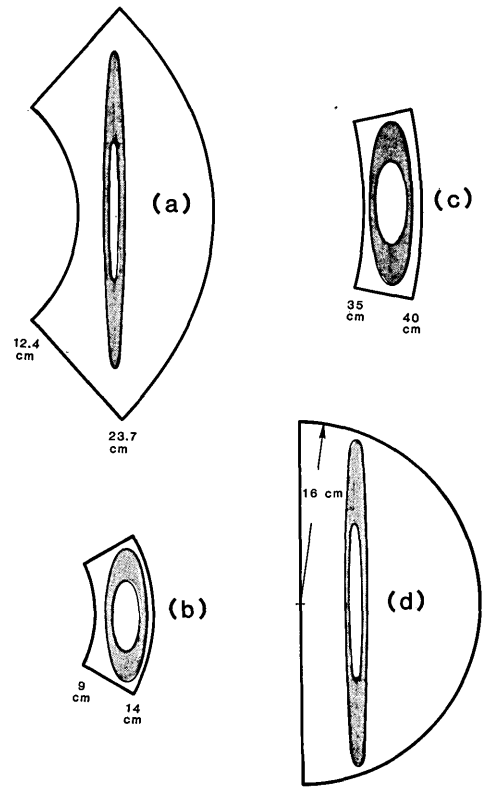

Fig. 2. Camera mirror choices: (a) a Wolter-Schwarzschild (W-S) type II accepting the beam from a 63.5° blaze angle echelle; (b) a W-S type II accepting the beam from a 30° echelle; (c) a W-S type I accepting the beam from a 45° echelle; (d) a normal incidence f10 paraboloid accepting the beam from a 63.5° echelle. All cameras are drawn to the same scale. Radii of curved perimeters are indicated.

1 indicated a 200-cm focal length (190 cm indicated in paper 2) and a 140-cm front-to-focus physical length. This camera must be large enough to accommodate the elongated elliptical beam exiting the 63.5° echelle, being 1.65 × 29.6 cm for the preliminary design of paper 1 and 2.0 × 31 cm for the detailed designs of paper 2. Within the constraint of a 140-cm physical length, the optimum W-S II solution is a scaled-up version of the survey telescope presented in Ref. 7. Using the notation adopted there, the dimensionless parameters are C = 165.0, R = 3.2, α_{min} = 0.0621, and α_{max} = 0.1190. The diameter of the primary is 47.4 cm, and its mirror length is ~58 cm. Paper 2 shows that this choice has the widest field of the designs studied (e.g., curve V in Figs. 4–7 of that paper that represent the same design scaled-up further to a 1-m diam). Area-weighted graze angles of reflection are 12.5° for the primary and 10.2° for the secondary.

Given the illumination shown in Fig. 2(a), we have performed numerical ray traces of this optic to determine its off-axis imaging properties. Figure 3 displays these results accompanied by the image of a 1- sec of arc entrance aperture (point response) following distortion by the conical echelle. The latter image is 3.5 × 56 sec of arc, assumed in paper 1 to be larger than the camera aberrations within a field of 20 × 20 min of arc. Paper 2 claimed a 30-min of arc field within which the camera

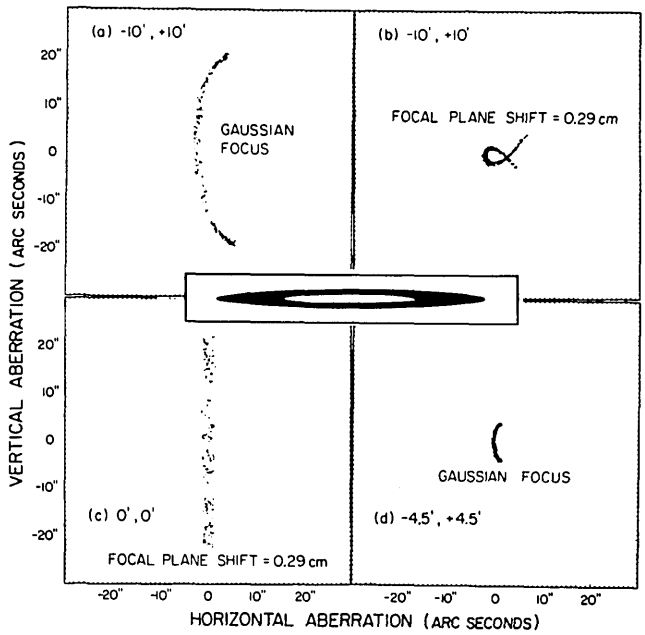

Fig. 3. Ray traces of the optimized W-S type-II camera mirror. The primary is illuminated by 500 rays placed randomly within the ellipse of Fig. 2(a). (a)–(d) show the spot diagrams at various off-axis angles and detector displacements. The central insert is the diffracted ellipse (3.5 × 56 sec of arc) within which the camera aberrations must lie.

aberrations were assumed small in comparison to the 2.1 × 35 sec of arc image. However, Fig. 4 illustrates that the major axis of this image ellipse must be normal to that of the equally distorted spatial beam. The image represents an uncertainty in angle and the beam represents an uncertainty in position; to conserve phase space (Liouville's theorem), the two must be inversely related. Since the camera aberration is found to be in the direction of the spatial beam elongation, independent of the off-axis angle, the important result is a mismatch between the direction of image elongation and the direction of maximum camera aberration. This is shown in Fig. 3(a). At the corner of a 20 × 20-min of arc field, the camera aberration is a factor of 12 too large (even worse if one correctly requires the camera aberration to be no more than half of the assumed total aberration).

Displacing the detector can greatly reduce this aberration [Fig. 3(b)] but only at the expense of defocusing the central image by such a large amount [Fig. 3(c)] that no net improvement is achieved. In principle, a curved detector can maintain both a stigmatic central image and the optimum off-axis response of Fig. 3(b), but the required radius of curvature is found to be 1.15 cm. In practice, this is prohibitively small by an order of magnitude. We note that such a high degree of focal curvature is in contradiction to the assertion in paper 2 of a flat focal plane over a 0.5° field. The largest usable field is ~9 × 9 min of arc [Fig. 3(d)], at the corners of which the aberrations have grown to a factor of 2.5 larger than the assumed 3.5 × 56-sec of arc image. This degrades the resolution from 10,000 at the center to

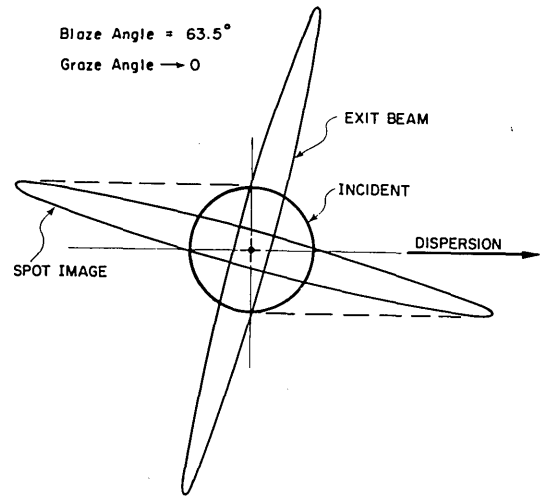

Fig. 4. Geometrical distortions in conical diffraction. The incident beam and incident image are both circular. The diffracted beam and image are elliptical and perpendicular to each other. The area enclosed by the circle is equal to that enclosed by the ellipse. Distortions are the same for graze angles $\lesssim 20°$.

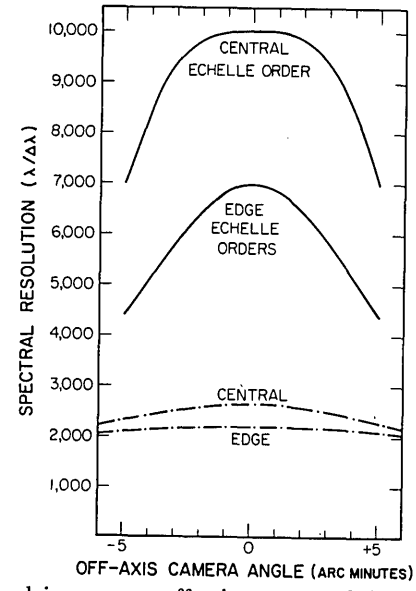

Fig. 5. Resolving power vs off-axis camera angle in the direction of echelle dispersion. The data are taken from Fig. 3. Solid curves represent a design which covers a 3% bandpass; dot–dash curves represent a design which covers a 25% bandpass.

~4000 at the edges of the spectrum as plotted in Fig. 5 for two sample echelle orders. Since this is achieved over a solid angle only one-fifth of the assumed 20 × 20-min of arc field, the spectrum covered by the enclosed 2-D echellogram decreases by a factor of 5.

A consideration which was neglected in papers 1 and 2 is echelle ripple. It was assumed that only one echelle order would be used for any given wavelength [e.g., Eqs. (14) and (15) of paper 1, or Eq. (11) of paper 2]. However, this has the undesirable effect of introducing a 50% peak-to-peak ripple in the theoretical echelle efficiency (Fig. 6). While this large effect was noted in

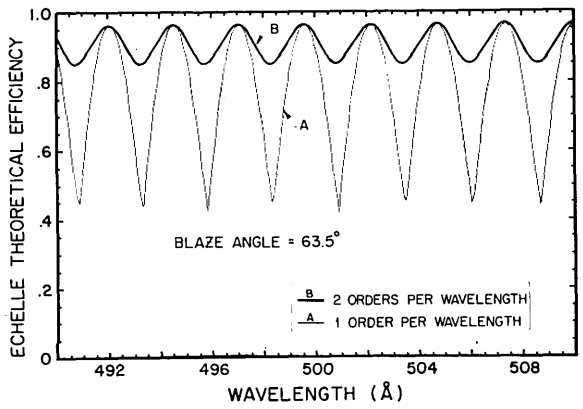

Fig. 6. Theoretical relative diffraction efficiency for an echelle. The light curves result from use of only the nearest echelle order at a given wavelength. The dark curves result from summing two adjacent echelle orders.

paper 2, no provisions were made to reduce it or to include the mean efficiency value (70%) into the performance estimates. We take the former approach, as the use of two echelle orders per wavelength is a standard procedure[8] which leads to only a 15% ripple and an average efficiency of 90% (Fig. 6). The important effect is a reduction by a factor of 2 in the number of echelle orders which can fit with a given field. A corrected version of Eq. (15) in paper 1, therefore, reads

$$W = 4(\sin\gamma)(\tan\beta)/n_{\min}, \quad (1)$$

where W is the angular width of the lowest echelle order $n_{\min}$, γ is the echelle graze angle (10°), and β is the echelle blaze angle (63.5°). The same correction applied to Eq. (14) (paper 1) or Eq. (11) (paper 2) results in $W = 2\lambda/(d\cos\beta)$.

Including all the above effects, we find that echelle orders n = 394–406 cover a 3% range in wavelength within a 9 × 9-min of arc field. Each echelle order is separated by a dark space of twice their thickness.[1] Since no one aberration is negligible (even the detector pixel sizes are equal to half of the minor axis of the central images), the parameters used in this analysis are nearly optimized given the constraints of overall system size, mirror figure, and detector pixel size. We, therefore, find a factor of 10 error in the proposed spectral coverage of a 30% wavelength range, and a factor of 2 decrease in the spectral resolution at the edges of the useful spectrum. Table I summarizes these results.

In the case of the design variation of paper 2, the 0.68-sec of arc collecting mirror results in a smaller spot, ~2.1 × 35 sec of arc. The useful camera field decreases to 7 × 7 min of arc, and thus the resulting bandbass decreases by a factor of 1.75 to 1.7% as indicated in Table I. This represents a factor of 9 smaller bandpass than reported in paper 2. In addition, the assumed 20-μm detector pixels are now equal to the minor axis of the image ellipses, degrading the peak resolution by $\sqrt{2}$. We also note that a 10° graze angle echelle, which is assumed in calculations of efficiency (Sec. III), translates to a collecting mirror with a 0.5-sec of arc figure.

A decrease in the amplification ratio c of the stellar image (i.e., a larger collimator) can increase the bandpass through a smaller required echelle blaze angle. The distortions of both the beam and the focal plane images decrease with the result of a wider camera field. However, larger collimators lead to proportionately longer spectrographs. The total instrument length is already quite large (5.9 m) as is the diameter of the camera primary (~0.5 m). Section IV discusses a more convenient modification which widens the spectral bandpass.

A trade-off between spectral resolution and bandpass is an inherent property of systems containing a camera mirror. Starting with the assumption of a 25% bandpass, we have found the spectral resolution decreases to the range $\lambda/\Delta\lambda$ = 2000–2500 (Fig. 5). Such a system would contain a lower-dispersion echelle (β = 30°) and

Table I. Performance Estimates for a Proposed Class of EUV Echelle Spectrometers

Design	Source of data	$\lambda/\Delta\lambda$[a]	$\lambda_{max}/\lambda_{min} - 1$	A_{eff}/A_{geom}[b] 200 Å (%)	500 Å (%)	1200 Å (%)	Total[c] length (m)
All-grazing echelle	Cash (Ref. 1)	10,000	0.30	0.5	1.5	1.2	4.7
As above	This work	4000–10,000	0.03	0.1	0.45	0.3	4.7
All-grazing echelle[d]	McClintock & Cash (Ref. 2)	20,000	0.15	0.5	1.5	1.2	5.9
As above	This work	8000–14,000	0.017	0.1	0.45	0.3	5.9
Lower dispersion echelle	This work	2000–2500	0.25	0.1	0.45	0.3	3.8
Type-I camera	This work	4000	0.30	0.1	0.45	0.3	4.2
Steeper echelle graze	This work	8000	0.15	0.05	0.22	0.15	3.8
Smaller slit	This work	6000	0.15	0.05	0.22	0.15	4.2
Normal Inc. camera	This work	10,000	0.40	N/A	0.15	0.10	5.5
0.5 sec of arc Collect. mirr. Norm. Inc. Cam.	This work	20,000	0.40	N/A	0.15	0.10	6.7
0.05 sec of arc Normal Inc. Collect. Mirr.	This work	30,000	~0.2	N/A	0.15	0.10	8.1

[a] Assumes a 1-sec of arc grazing collecting mirror, except where othewise noted.
[b] Includes a 30% detector efficiency, gold-coated optics, 10° graze angles (except where noted). Each wavelength is assumed to be at peak blaze of cross disperser. Echelle ripple not included.
[c] Length includes the spectrograph plus a 1-m diam collecting mirror.
[d] Assumes a 0.68-sec of arc collecting mirror. Designs tailored to operate at the different wavelengths (200, 500, 1200 Å) are compared with those from Tables I and II of Ref. 2. Only design difference is the choice of groove density and blaze angle for the cross disperser.

a shorter camera mirror (physical length = 72 cm, focal length = 97 cm) of which only a small section of its circumference is illuminated [Fig. 2(b)]. The 1-sec of arc entrance aperture represents an 8 × 24-sec of arc image after diffraction by the echelle; orders 70–90 are placed within a 14 × 14-min of arc camera field. Table I includes this design. Compared with the original design, the camera is 68 cm shorter, and the echelle is 25 cm shorter, thus the total instrument length decreases by ~0.9 m. This is an example of the trade-off between system length and resolution.

III. Efficiency

The net efficiency of the instrument (spectrometer plus collecting mirror) is equal to that fraction of the incident light which is detected:

$$A_{\text{effective}}/A_{\text{geometric}} = R \times \epsilon_E \times \epsilon_C \times b^2 \times QE, \qquad (2)$$

where R is the net reflectance of the eight-bounce system, ϵ_E and ϵ_C are the theoretical relative diffraction efficiencies of the two gratings, and b is the fraction of theoretical grating efficiency which is experimentally recovered. The latter ratio is also referred to as the groove efficiency.[10] QE is the detector quantum efficiency. For all calculations we will assume a detector QE of 30%.[9] As was done in papers 1 and 2, we will ignore variations in ϵ_E (echelle ripple) and any decline in ϵ_C away from the peak blaze. In paper 1, several factors of Eq. (1) were grouped together requiring $b\epsilon_E \simeq b\epsilon_C = e$, where e is the relative diffraction of efficiency of a grating.

Using two echelle orders per wavelength and neglecting the rapid fluctuations in efficiency due to echelle ripple, Fig. 6 reveals that the mean diffraction efficiency is theoretically $\epsilon_E = 0.9$ for the echelle. For an in-plane mounted cross-disperser (paper 1), we also calculate a peak blaze of $\epsilon_C = 0.8$. This is not 100%, due to groove shadowing for the in-plane mount. However, we shall assume a peak at 100% (e.g., the off-plane disperser mount of paper 2). Using $e = 0.65$ from paper 1, we thereby find $b \simeq 0.7$. Such high groove efficiencies can be obtained in the EUV/FUV by high-quality ruled gratings.[10] Grazing incidence measurements in the soft x-ray[3,5] have obtained groove efficiencies of ~60%, while published EUV measurements have recovered 70% of the theoretical diffraction efficiencies in both classical[4,11] and conical[4,5] mountings. Thus, we assume $b = 0.7$ for grazing incidence gratings operating in the 100–1200-Å wavelength range and thereby adopt the diffraction efficiency assumptions of papers 1 and 2.

Using the efficiency curves reported in Fig. 10 of paper 1 or in Fig. 12 of paper 2, the net reflectance is inferred to be R = 6–16% longward of 200 Å. This requires an effective single-bounce reflectance of 70–80%. The reflection graze angles assumed in papers 1 and 2 were 10°. Although the latter designs require a 12.5° echelle graze angle (Table I of paper 2), and in both cases the camera primary graze angle was also found to equal 12.5° (Sec. II), our efficiency estimates will for clarity assume an optimistic 10° graze angle for each of the eight surfaces. Figure 2 of paper 2 indicates the reflectance of gold at 10° is 70–75% for $\lambda > 400$ Å. Paper 1 suggested that the assumed reflectance values were inferred from one set of data reported by Malina and Cash.[12] Figure 7 shows the reflectance measured by several authors for gold,[13] platinum,[14] and rhodium,[15] revealing an average reflectance of 60–65% over the wavelength range from λ = 200–1200 Å. At best, platinum mirrors peak at 65–70% in the 300–600-Å wavelength range. The results shown in Fig. 7 are corroborated by other published data.[16] It is evident that the 70–80% reflectances assumed for the calculations in papers 1 and 2 are consistently too high by 20–30% in relative magnitude. While this is not a dramatic correction factor for a single reflection, it overestimates the eight-bounce reflective throughput by factors of from $(1.2)^8$ to $(1.3)^8$ = factors of 4–8.

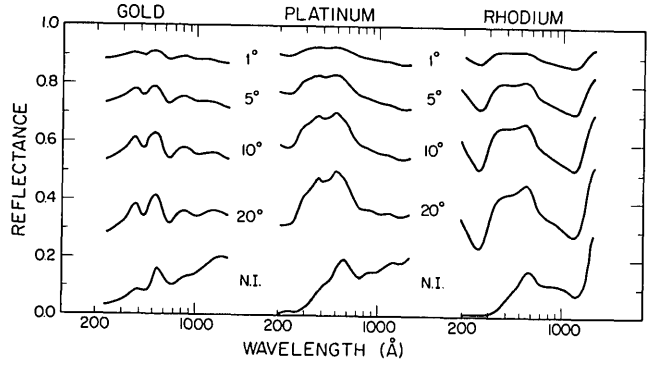

Fig. 7. Reflectance vs wavelength in the range λ = 230–1200 Å. Data taken from published multiangle reflectance measurements. *N.I.* signifies normal incidence.

This large overestimate is offset in small amounts by taking into account the induced polarization from upstream reflectances in the optical train. For surfaces oriented in a parallel configuration as is the case for all surfaces of revolution sharing the same axis of revolution, the use of unpolarized reflection coefficients for all bounces will underestimate the net reflectance. In the event where each surface is at right angles to the preceding one, however, neglect of induced polarization will overestimate the net reflectance. These effects can be understood by considering a two-bounce system, where the correct reflectance is obtained by multiplying each linear polarization separately and then averaging. The triangle inequality then requires

$$(R_p^2 + R_s^2)/2 > [(R_p + R_s)/2]^2 > (R_pR_s + R_sR_p)/2, \qquad (3)$$

where R_p and R_s are positive, and $R_p \neq R_s$. This effect becomes increasingly important near the Brewster angle for which $R_s \gg R_p$. For the adopted graze angles of 10°, the ratio of the single-bounce reflectances is ~1.06 at 100 Å, 1.33 at 200 Å, 1.3 at 500 Å, and 1.8 at 900 Å.

In the proposed eight-bounce system, the first four surfaces are locally parallel (surfaces of revolution), and the last four surfaces are approximately parallel, however, the boundary consists of a plane grating which intercepts all angles from the upstream surfaces of revolution. For this configuration we find a net reflectance of

$$R = [(R_p^4 + R_s^4)]^2. \quad (4)$$

Note that this is larger than that obtained from the naive formula which neglects induced polarization: $[(R_p + R_s)/2]^8$. However, the net increase is only a factor of 1.2 at 500 Å and a factor of 2.2 at 1200 Å. Using the reflectance data of gold from Canfield *et al.*,[13] our results for the net efficiency of the proposed instrument are presented in Table I. Using the same detector QE (30%), we obtain an average of a factor of 4 lower efficiency than that estimated in papers 1 and 2. Results being reported by Werner[17] factored by our assumed detector efficiency are in very close agreement with the values in Table I. If only one echelle order per wavelength is used, we can increase the bandpasses by a factor of 2 over that found in Sec. II, but the efficiency then decreases to equal only one-fifth of that estimated in papers 1 and 2. The efficiencies reported in Table I assume the starlight is unpolarized prior to entering the collecting mirror. In the event that the incident radiation is 100% linearly polarized, we find a factor of 2 increase to a factor of 3 decrease in efficiency depending on the direction of polarization.

IV. Modifications to the Proposed Design

As shown in Sec. II, the resolution and spectral coverage of the proposed design are fundamentally limited by the aberrations from the grazing incidence camera mirror. Our first goal was to determine if the proposed resolution ($\lambda/\Delta\lambda = 10{,}000$) and spectral coverage (30%) could be obtained without further decreases in efficiency. This requires the geometry of all-grazing incidence to be maintained and the use of the echelle in conical diffraction.

A. Wolter-Schwarzschild Type-I Camera

We have ray-traced type-I W-S mirror systems[18] over a large parametric grid from graze angles of 0.5–16° and have found their fields are typically wider than those of type-II construction. (Paper 2 suggested use of a type-I camera mirror to achieve a 1° field of view.) However, the required physical length for a type-I camera is approximately equal to its effective focal length. If dominated by detector pixels, use of a Type I camera would then require a longer instrument. However, it has been shown in Sec. II that the aberrations of a type-II camera dominate the resolution. It was also shown that, if a 25% bandpass is desired with a type-II mirror, the echelle blaze angle is reduced to 30° and the resulting spectral resolution to $\lambda/\Delta\lambda = 2000$–2500. The images at this resolution are no longer highly elliptical [Fig. 2(b)] and can be resolved with a camera focal length as short as 80 cm. In effect, the large aberrations found for a type-II mirror make the type I a better choice. Its wider field can be used to obtain somewhat higher resolution (equally limited by detector pixels and aspect) and a larger bandpass.

For example, using a 45° blaze angle echelle, the on-axis spectral resolution would be 5000. Figure 2(c) shows the illuminated section of the camera mirror, which is a small circumference of a large radius primary.

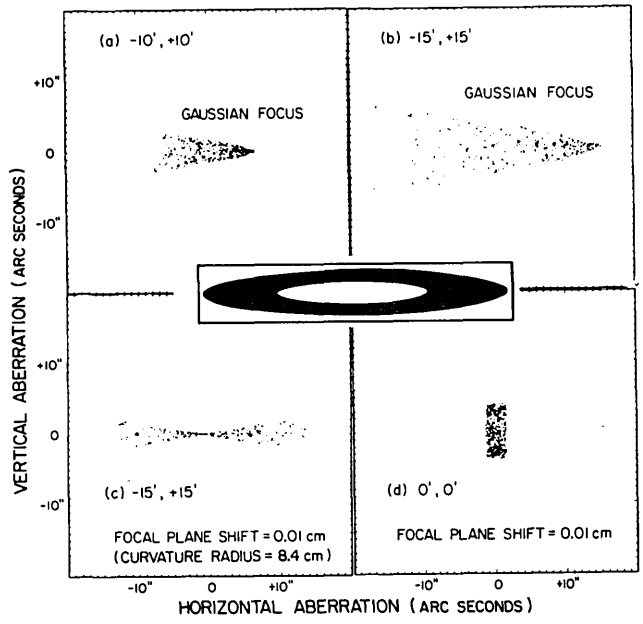

Fig. 8. Ray traces of an optimized W-S type-I camera. The primary is illuminated by 500 rays placed randomly within the ellipse of Fig. 2(c). The optimum detector curvature is 8.4 cm.

Using the notation of Ref. 6, the parameters for this camera are $F = 67$ cm, $F/g = 1.25$, $\beta^* = 0.5496$, and $\beta_{max} = 0.6398$. Note that β is not to be confused with our duplicate use of that symbol for the echelle blaze angle. This mirror is quite large having an 80-cm diam primary. The area-weighted graze angles are 7.8° for the primary and 9.2° for the secondary. Due to the short camera focal length, the assumed 15-μm detector pixels degrade the resolution from 5000 to 4000.

Figure 8 presents the results of numerical ray tracings. Defocusing of the on-axis image by 0.01 cm is found to be acceptable and results in a field of 30 × 30 min of arc within which the camera mirror aberrations are comparable with the 6 × 32-sec of arc ellipse emerging from the echelle. Moreover, the optimum focal surface curvature is 8.4 cm and attainable with imaging detectors. If the resolution of 4000 is not to significantly degrade, the camera aberrations must be contained well within the diffracted ellipse images implying a field of ~22 × 22 min of arc. By use of Eq. (1) we find $n_{min} = 92$. Given the previous stated requirement on the separation of echelle orders, thirty orders fit within the 22-min of arc field. Thus a 30% bandpass is achieved, but only at a resolution of 4000. Due to detector pixels, higher spectral resolution is unavailable unless the system length is increased beyond 4.2 m.

B. Efficiency/Resolution Trade-Offs

We next attempted to increase the resolution while maintaining grazing incidence and thus the capability for wavelengths in the XUV region of $\lambda \sim 100$–500 Å. Possible solutions include the use of larger graze angles and the use of an in-plane echelle. The former procedure directly increases the dispersive power without affecting the sizes of the diffracted beam or the focal

plane images, while the use of in-plane diffraction results in smaller beam or images. In both cases, however, the absolute grating efficiency decreases due either to lower reflectance or lower diffraction efficiency. For example, the resolution may be increased by a factor of 2 compared with the previous W-S I design from $\lambda/\Delta\lambda$ = 4000–8000 by use of a 20° graze angle in conical diffraction. However, from Eq. (1), this results in a factor of 2 increase in the value of the minimum echelle order n_{min}, since the camera field of view W is the same. The same number of echelle orders thus results in only one-half of the spectral coverage as before, or 15%. In addition, the efficiency decreased by a factor of 2 due to the lower reflectance (Fig. 7). This solution appears in Table I.

In principle, the spectral resolution may be also increased by overilluminating a slit which is smaller than the size of the stellar image. However, this has the obvious side effect of lowering the efficiency. In addition, the effect of detector pixels on the resolution is larger. For example Table I shows a 50% increase in resolution (type-I camera) but a factor of 2 decrease in efficiency. A factor of 2 smaller bandpass also results from the smaller camera field which must accommodate the thinner wavelength images.

Figure 7 also shows that reflectances can be increased by tailoring the coatings for a specific bandpass. However, to obtain a factor of 2 increase in efficiency for the eight-bounce instrument, at least all the six reflections within the spectrometer would need to be used exclusively in such regions where the enhancement is desired. An average reflectance of 60–65% over the region λ = 200–1200 Å is, therefore, a more reasonable assumption.

C. Normal Incidence Optics

It is well known that normal incidence optics provide superior off-axis imaging and thus wider fields than grazing incidence optics. A single-element normal incidence paraboloid, with a 15% reflectance (Fig. 7) has approximately one-third the efficiency of a two-element grazing incidence mirror (65 → 65%). It could operate with this efficiency at any EUV/FUV wavelength longward of ~400 Å. In addition, if SiC mirror[19] or grating[20] coatings can be fabricated to reflect at twice this efficiency, the degradation compared to grazing incidence would be only ~50%, except for the loss of capability to $\lambda \leqslant 400$ Å. Another possibility is the use of multilayer coatings,[21,22] which can reflect at wavelengths <400 Å over the 10% bandpasses at which this design class is found to operate.

In paper 2 the authors have proposed such hybrid designs including a normal incidence echelle or a Wadsworth cross-disperser/camera configuration. In Fig. 9 we have ray traced only the case of a normal incidence f10 paraboloidal camera mirror which is illuminated [Fig. 2(d)] by a high-dispersion grazing echelle. This should yield an upper limit to the imaging expected for the Wadsworth design. This requires a longer instrument (300 cm from camera to detector) than previously constrained. We find a 40 × 40-min of arc field

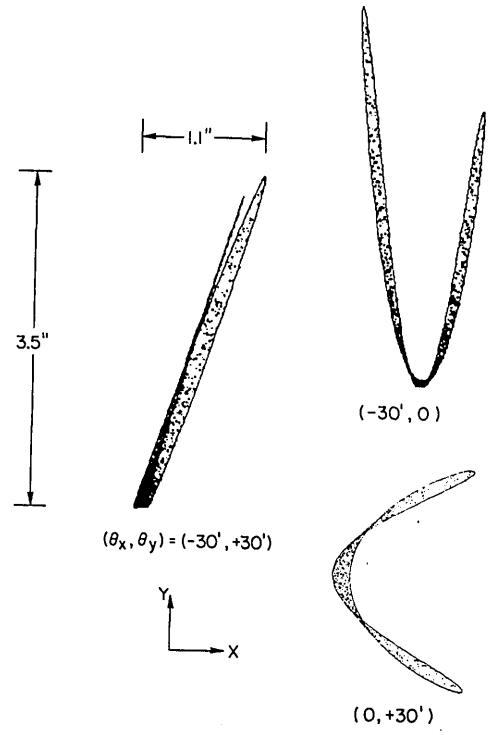

Fig. 9. Ray traces of a normal incidence f10 paraboloid illuminated by 1000 rays placed randomly within ellipse of Fig. 2(d). Dispersed wavelengths from the echelle extend to 56 sec of arc in the horizontal direction and 3.5 sec of arc in the vertical direction. The dimensions of one of the spot diagrams are indicated.

of view within which the camera aberrations are acceptably small. We thereby estimate a 50% bandpass, which employs echelle orders n = 120–180. However, over such large bandpasses, one must take account of the uneven spacings between echelle orders. In the simple case, where cross-dispersion provides equal angular dispersion per unit wavelength, separation of the closest echelle orders requires

$$2(\lambda/\Delta\lambda)(\lambda_{max}/\lambda_{min}) \log_e(\lambda_{max}/\lambda_{min}) = (W/\Delta\theta)^2/c^2/(s+1), \quad (5)$$

where s is the ratio of minimum dark space to echele order thickness, $\Delta\theta$ is the figure of the collecting mirror, c is the beam concentration provided by the collimator, and W is the camera field as used in Sec. II. Using $\Delta\theta$ = 1 sec of arc, c = 14, s = 2, W = 40 sec of arc, and requiring $\lambda/\Delta\lambda$ = 10,000, we find $\lambda_{max}/\lambda_{min} - 1$ = 40%. The aberrations from detector pixels are negligible, since the 300-cm focal length camera produces ellipses whose minor axes are 52.5 μm.

Table I also includes the result assuming a 0.5-sec of arc mirror. To resolve the smaller images (1.75 × 28 sec of arc) the camera focal length must be $\sqrt{2}$ larger, or 420 cm. In calculating the instrument length using a normal incidence camera, we have assumed the detector is placed at the distance of the spectrograph entrance slit from the camera. Thus using a 2.5-m distance from the collecting aperture to the slit (paper 1), this design is 6.7 m in total length.

Including a 15% normal incidence reflectance, Table I reports efficiencies of ~0.1% for this hybrid design.

This can rise by a factor of 1.3 if the camera and cross disperser can be combined into a normal incidence Wadsworth grating which attains 60% of its theoretical EUV efficiency, or ~9%.

D. Normal Incidence Collecting Mirror

Large aperture grazing incidence mirrors with 0.5–1-sec of arc figures represent technology which is being currently developed.[23] However, conventional normal incidence mirrors can presently provide diffraction-limited performance for apertures as large as 2.4 m in diameter.[24] Using a 1-m diam paraboloid, the diffraction limit at λ1200 Å is only ~0.025 sec of arc. Even if relaxed to 0.05 sec of arc, this represents an order of magnitude improvement over what can be expected from future grazing incidence mirrors.

One can take advantage of such mirrors to improve the performance of an all-grazing incidence version of the proposed spectrometer in several areas. First, if the collimator is made a factor of 5 smaller ($c = 70$), the aspect on the grating system is still a factor of 4 smaller than with a 1-sec of arc mirror. This increases the dispersive resolution by a factor of 4 to $\lambda/\Delta\lambda = 40{,}000$ with a $\beta = 63.5°$ echelle at a 10° graze angle. If the camera's focal length is made 4 m long, the resolution will be limited equally by aspect and by 15-μm detector pixels at $\lambda/\Delta\lambda \simeq 30{,}000$. Due to the factor of 5 smaller beam, this camera will have a field of view which is found to be approximately the same factor larger in area. In this way, we estimate that a 20% bandpass can be covered at this resolution using a type-II camera mirror.

However, such designs are quite long. For example, a 1-m diam prime focus $f5$ mirror requires 5 m to focus. The 4-m effective focal length grazing incidence camera can optimistically fit within a 2.8-m physical length, and the collimator/gratings system is small (33 cm) due to the high concentration ratio. The total instrument length is then estimated to be 8.1 m. In addition, fine aspect and pointing systems are required to prevent degradation of the assumed 0.05-sec of arc mirror image.

V. Conclusions

We have analyzed the class of multibounce grazing spectrometers proposed by Cash[1] and by McClintock and Cash[2] and have found performance values significantly lower than asserted by these authors. Modifications to the proposed designs have been investigated and found not to alter this conclusion. In particular,

(1) the use of a type-I camera mirror improves the bandpass but cannot attain the proposed resolution within the proposed physical instrument envelopes.

(2) the introduction of normal incidence optics significantly increases the resolution, but requires long spectrograph lengths. In addition, the efficiency is lowered by an additional factor of 2–3, and the capability for wavelengths shortward of ~400 Å is lost.

The development of echelle spectrometers to grazing incidence optics is an important area of current research. The proposed adaptation of a conventional multibounce design to grazing incidence benefits largely from the use of the echelle in conical diffraction. However, the resulting eight-bounce system provides very low efficiency. The design also maintains a camera mirror, which historically was designed for use in normal incidence spectrometers. At grazing incidence, the aberrations introduced by this optic severely limit the attainable spectral resolution and bandpass available at a given setting of the cross disperser.

We specifically note that grazing incidence designs exist which contain significantly fewer reflections and do not use camera mirrors (or curved gratings).[25,26] Such designs thus avoid the dominant limitations inherent in the design class discussed above.

We thank C. Martin for helpful discussions and for originally suggesting the presence of camera aberrations. This work was supported by NSF grant INT-8116729 and NASA grant NAG 5-420.

Patrick Jelinsky also holds an appointment with the University of California, Department of Physics; Stuart Bowyer also holds an appointment with University of California, Department of Astronomy.

References

1. W. Cash, "Echelle Spectrographs at Grazing Incidence," Appl. Opt. **21,** 710 (1982).
2. W. E. McClintock and W. Cash, "Grazing Incidence Optics: New Techniques for High Sensitivity Spectroscopy in the Space Ultraviolet," Proc. Soc. Photo-Opt. Instrum. Eng. **331,** 12 (1982).
3. W. Werner, "X-Ray Efficiencies of Blazed Gratings in Extreme Off-Plane Mountings," Appl. Opt. **16,** 2078 (1977).
4. M. Neviere, D. Maystre, and W. R. Hunter, "On the Use of Classical and Conical Diffraction Mountings for XUV Gratings," J. Opt. Soc. Am. **68,** 1106 (1978).
5. W. Cash and R. Kohnert, "Very High X-Ray Efficiency From a Blazed Grating," Appl. Opt. **21,** 17 (1982).
6. Final Report of the Working Group for the Far Ultraviolet Spectroscopic Explorer, NASA headquarters publication (April 1983).
7. M. Lampton, W. Cash, R. F. Malina, and S. Bowyer, "Design, Fabrication and Performance of Two Grazing Incidence Telescopes for Celestial Extreme Ultraviolet Astronomy," Proc. Soc. Photo-Opt. Instrum. Eng. **106,** 93 (1977).
8. B. E. Turnrose and C. A. Harvel, *International Ultraviolet Explorer Image Processing Information Manual* (1979).
9. C. Martin and S. Bowyer, "Quantum Efficiency of Opaque CsI Photocathodes With Channel Electron Multiplier Arrays in the Extreme and Far Ultraviolet," Appl. Opt. **21,** 4206 (1982).
10. B. W. Bach, "Vacuum Ultraviolet Gratings," Proc. Soc. Photo-Opt. Instrum. Eng. **240,** 223 (1980).
11. J. Edelstein, M. C. Hettrick, S. Mrowka, P. Jelinsky, and C. Martin, "Extreme UV Measurements of a Varied Line-Space Hitachi Reflection Grating: Efficiency and Scattering," Appl. Opt. **23,** 3267 (1984); submitted for publication.
12. R. F. Malina and W. Cash, "Extreme Ultraviolet Reflection Efficiencies of Diamond-Turned Aluminum, Polished Nickel, and Evaporated Gold Surfaces," Appl. Opt. **17,** 3309 (1978).
13. L. R. Canfield, G. Hass, and W. R. Hunter, "The Optical Properties of Evaporated Gold in the Vacuum Ultraviolet from 300 Å to 2000 Å," J. Phys. **25,** 124 (1964); W. R. Hunter, Naval Research Laboratory; private communication (1982).
14. W. R. Hunter, D. W. Angel, and G. Hass, "Optical Properties of Evaporated Platinum Films in the Vacuum Ultraviolet from 220 Å to 150 Å," J. Opt. Soc. Am. **69,** 1695 (1979).
15. J. T. Cox, G. Hass, and W. R. Hunter, "Optical Properties of Rh Films in VUV, J. Opt. Soc. Am. **61,** 360 (1971).

16. J. H. Weaver, C. Krafka, D. W. Lynch, and E. E. Koch, "Optical Properties of Metals," Vols. I and II, DESY F41 Hasylab 81/01 and 81/05 (1981).
17. W. Werner, "Comparison of Various Grazing Incidence Spectrometer Designs Based on Conical Diffraction," Appl. Opt. (1984); submitted for publication.
18. R. F. Malina, S. Bowyer, D. Finley, and W. Cash, "Wolter-Schwarzschild Optics for the Extreme Ultraviolet: The Berkeley Stellar Spectrometer and the EUV Explorer," Opt. Eng. 19, 211 (1980).
19. P. S. M. Davila, R. A. M. Keski-Kuha, J. F. Osantowski, T. T. Saha, and G. A. Wright, "Design and Technology Considerations for the Far Ultraviolet Spectroscopic Explorer (FUSE) Telescope," Proc. Soc. Photo-Opt. Instrum. Eng. 445, (1983).
20. D. L. Windt and B. Bach, "Ion Beam Deposited Silicon Carbide on Glass Optics and Replica Gratings," Appl. Opt. 23, (1984); submitted for publication.
21. R. Stern, B. Haisch, E. Joki, and R. Caturi, "Normal Incidence Multilayer Mirrors for Extreme Ultraviolet Astronomy," Proc. Soc. Photo-Opt. Instrum. Eng. 445, 347 (1983).
22. E. Spiller, A. Segmuller, J. Rife, and R.-P. Haelbich, "Controlled Fabrication of Multilayer Soft-X-Ray Mirrors," Appl. Phys. Lett. 37, 1048 (1980).
23. M. V. Zombeck, "AXAF, A Permanent Orbiting X-Ray Observatory: Telescope and Instrumentation Plans," Harvard-Smithsonian Center for Astrophysics preprint series no. 1658.
24. D. N. B. Hall, Ed. "The Space Telescope Observatory," Special Session of Commission 44, IAU Eighteenth General Assembly, Patras, Greece (Aug. 1982); NASA publication CP-2244.
25. M. C. Hettrick and S. Bowyer, "Variable Line-Space Gratings: New Design for Use in Grazing Incidence Spectrometers," Appl. Opt. 22, 3291 (1983).
26. M. C. Hettrick, "Aberrations of Varied Line-Space Grazing Incidence Gratings in Converging Light Beams," Appl. Opt. 23, 3221 (1984).